Petroleum Science 22 (2025) 756–770

Contents lists available at ScienceDirect

Petroleum Science

journal homepage: www.keaipublishing.com/en/journals/petroleum-science

Original Paper

Experimental study of microscopic oil production and CO_2 storage in low-permeable reservoirs

Ming-Xing Bai [a, b], Zhi-Chao Zhang [a, b, *], Er-Long Yang [a, b], Si-Yu Du [a, b]

[a] Northeast Petroleum University, Daqing, 163318, Heilongjiang, China
[b] Key Laboratory of Ministry of Education for Enhanced Oil Recovery, Northeast Petroleum University, Daqing, 163318, Heilongjiang, China

ARTICLE INFO

Article history:
Received 2 September 2024
Received in revised form
15 December 2024
Accepted 15 December 2024
Available online 18 December 2024

Edited by Yan-Hua Sun

Keywords:
CO_2 disaplacement
Oil recovery
CO_2 sequestration
CO_2-induced reactions
In-situ nuclear magnetic resonance

ABSTRACT

Enhanced CO_2 sequestration (ECS) within low-permeable reservoirs during CO_2-enhanced oil recovery (CO_2-EOR) processes has gained significant interest, primarily driven by the need to mitigate the greenhouse effect caused by excessive CO_2 emissions. In this work, the in-situ nuclear magnetic resonance (NMR) is applied to investigate the oil production and CO_2 sequestration within the micropores of low-permeable reservoirs. Additionally, the impact of CO_2–water–oil–rock reactions on CO_2-EOR and CO_2 sequestration is studied by analysis of the changes in minerals, pore structures, and wettability of cores by scanning electron microscopy (SEM), X-ray diffraction (XRD), and contact angle measurements with the experiments of CO_2–water–oil–rock interaction in the high-temperature and high-pressure (HT-HP) reactor. The results reveal that the residual water saturation (S_{wr}), CO_2 injection pressure, and the interaction among CO_2, water, oil, and rock all exerted a considerable impact on oil recovery and CO_2 sequestration. Compared with the oil recovery and CO_2 sequestration of the two oil-saturated cores (Core No. 2 and Core No. 3) after CO_2 injection, the accumulated oil recoveries of the two cores with $S_{wr} = 0.5$ are enhanced by 1.8% and 4.2%, and the CO_2 sequestration ratios are increased by 3% and 10%, respectively. Compared with the CO_2–water–rock that occurred in oil-saturated cores, the CO_2–water–rock reaction for cores ($S_{wr} = 0.5$) is more intense, which leads to the formation of more hydrophilic rock on pore surfaces after the reaction, thereby reducing the adhesion work of CO_2 stripping oil. The oil and water mixtures in pores also inhibit CO_2 premature breakthrough from cores, therefore expanding the swept volume of CO_2 in cores. Otherwise, oil recovery and CO_2 sequestration in small pores of cores are significantly improved with the rise in CO_2 injection pressure due to the enhanced driving pressure degree and also the improved mutual solubility and mass transfer between CO_2 and oil.
© 2024 The Authors. Publishing services by Elsevier B.V. on behalf of KeAi Communications Co. Ltd. This is an open access article under the CC BY-NC-ND license (http://creativecommons.org/licenses/by-nc-nd/4.0/).

1. Introduction

The idea of CO_2-EOR for low-permeable reservoirs was first proposed by Whorton et al. (1952). Extensive research and field trials demonstrated that the injection of either miscible or immiscible CO_2 into low-permeable reservoirs can effectively enhance oil recovery and mitigate the negative impact of CO_2 emissions (Koottungal, 2014; Wei et al., 2017). The Global Carbon Capture and Storage Institute (GCCSI) also released a research report highlighting the significance of CO_2 capture and sequestration within reservoirs in mitigating the negative effects of carbon emissions (Page et al., 2020). The incremental profitability from increased oil production by CO_2-EOR projects can help offset the expenses associated with CO_2 sequestration (Benson and Deutch, 2018). Hence, the coupled study of CO_2-EOR and CO_2 sequestration holds significant potential for simultaneously enhancing oil recovery and realizing CO_2 sequestration within hydrocarbon reservoirs (Kashkooli et al., 2022).

The earliest recorded project of CO_2-EOR integrated with CO_2 sequestration was conducted in the Weyburn oilfield situated in Canada. Consequently, the decline in formation pressure resulted in a decrease in oil production, from a peak of 45,000 barrels per day in 1964 to just 15,000 barrels per day by 1980 (Brown et al., 2017). To enhance oil recovery, CO_2 injection was implemented in 2000 with a consistent CO_2 injection rate of 5000 tons per day. After CO_2 injection, oil production of this oilfield increased significantly to

* Corresponding author.
E-mail address: zhangzhichao@nepu.edu.cn (Z.-C. Zhang).

https://doi.org/10.1016/j.petsci.2024.12.015
1995-8226/© 2024 The Authors. Publishing services by Elsevier B.V. on behalf of KeAi Communications Co. Ltd. This is an open access article under the CC BY-NC-ND license (http://creativecommons.org/licenses/by-nc-nd/4.0/).

25,000 barrels per day and sustained long-term stability of oil production (Preston et al., 2005). The CCUS-EOR project in the United States also achieved remarkable application results. Based on the report published by the Global CCS Institute in 2021, eleven large-scale CCUS-EOR industrial capture projects were successfully implemented in the United States, achieving 20.74 million tons of CO_2 storage capacity of underground storage structures (Global CCS Institute, 2021). Taking the Kelly Snyder oilfield in the Permian Basin as an example of the CO_2 miscible flooding project, by 2020, oil production in this block remained consistently stable for 16 years, resulting in a cumulative 24.56 million tons of oil increment and a cumulative CO_2 injection of 3.9×10^8 tons, thereby enhancing oil recovery by over 26% (Yuan et al., 2022). In 2021, 71 new CCUS demonstration projects were established for CO_2-EOR and CO_2 sequestration, aiming to achieve a CO_2 capture capacity of 150 million tons per year (Liu et al., 2023). The International Energy Agency (IEA) further assessed the promising potential of CCUS technology, predicting that by 2040, it will account for over 9% aimed at limiting global temperature rise to 2 °C. Additionally, CCUS technology is anticipated to contribute 15% towards the global objective of achieving net zero emissions of CO_2 by 2070 (IEA, 2020).

Following the promotion of the proposal of 'carbon neutrality' and the increasing demand for oil and gas resources, numerous scholars have undertaken research on CO_2-EOR and ECS. Bui et al. (2018) proposed the sequestration mechanism of CO_2 in reservoirs can be divided into structural sequestration, dissolution sequestration, residual sequestration, and mineral sequestration. Li et al. (2021) and Wang et al. (2022) conducted a series of comparative analyses to evaluate the impacts of continuous CO_2 injection, cyclic CO_2 injection, and CO_2 water-alternating gas (CO_2-WAG) injection on CO_2-EOR and ECS. The results indicated that the EOR effect of CO_2-WAG was the most effective, but the CO_2 storage capacity was the lowest in cores. The ECS effect of cores after cyclic CO_2 injection is better than that induced by CO_2-WAG and continuous CO_2 injection. Using the numerical simulation, Assef et al. (2019) evaluated the ECS effect in the Middle Bakken reservoir with cyclic CO_2 injection. They found the residual gas saturation (S_{rg}) within reservoirs increases during the cyclic CO_2 injection, which causes relative permeability hysteresis of CO_2, increasing the amount of CO_2 residual sequestration. Combined with particle swarm optimization algorithm analysis, Gao et al. (2021) proposed the equation of comprehensive effect factor (f) to optimize the CO_2-EOR and ECS during the whole process of CO_2 injection. By coupled optimization, they believe that in the early stage of CO_2 injection, the adjustment of production parameters is mainly for the target of EOR, and the amount of CO_2 sequestration within reservoirs is also relatively high at this stage. After CO_2 breakthrough from production wells, the rate of CO_2 injection should be appropriately reduced to improve the effect of CO_2-EOR and ECS. Le et al. (2022) evaluated the plugging behavior of CO_2 microbubbles in porous media through a series of experiments and believed that the injection of CO_2 microbubbles into heterogeneous reservoirs can effectively delay CO_2 breakthrough time, thus improving oil recovery. Ampomah et al. (2017) introduced an integrated numerical framework aimed at simultaneously optimizing the performance of enhanced oil recovery and CO_2 storage in reservoirs. Their findings revealed that when compared with the oil recovery and CO_2 storage of the base simulation scenario with a constant CO_2-WAG cycle of 3:1 for 20 years of injection, the oil recovery was enhanced by 28%, while the CO_2 storage capacity rose from 74% to 94% with the optimal scenarios. Yao and Li, 2009 and Hu et al. (2019) evaluated the impact of CO_2 immiscible/miscible flooding on the CO_2-EOR and ECS with the reservoir simulation method. The results suggest that CO_2 miscible flooding is more effective in enhancing oil recovery and CO_2 sequestration. Otherwise, CO_2 injection not only improves the permeability, and wettability of reservoir rock but also reduces the capillary resistance of cores with CO_2 injection, therefore enhancing the effect of CO_2-EOR and ECS (Arsyad et al., 2013; Rathnaweera et al., 2016; Zhang et al., 2018; Cui et al., 2021).

Currently, the main approach for the coupled study of CO_2-EOR and sequestration in reservoirs is by combining numerical simulation with optimization algorithms such as neural network algorithm, Monte Carlo simulation, etc, to systematically optimize the production parameters, CO_2 injection methods, bottom hole pressures, and well arrangement to maximize the CO_2-EOR and CO_2 sequestration of reservoirs (Ampomah et al., 2017; Khurshid and Afgan, 2021; Kashkooli et al., 2022). For example, Ampomah et al. (2017) used an art neural network optimization algorithm trained by numerical simulation data to optimize the CO_2-EOR and ECS. They found that under the optimal parameters, the predicted CO_2 sequestration percentage within reservoirs (Farnsworth field unit, Ochiltree County, and Texas) reaches 94%, and the oil recovery increases by 28% after 20 years of CO_2-water gas alternating injection (CO_2-WAG). However, rarely pay attention is considered to the coupled CO_2-EOR and sequestration in reservoirs with different water saturation at the microscale, as well as the impact of CO_2—water—oil—rock interaction on the effect of CO_2-EOR and ECS. Moreover, the conventional analysis (non-in-situ NMR, non-in-situ CT methods, etc.) for oil production in micropores of the core after CO_2 injection was mostly done by removing the core from the core gripper, which resulted in the redistribution of oil and gas in the pores of the core, causing significant experimental errors. Therefore, this paper presents the novel characterization method of in-situ nuclear magnetic resonance (NMR) to analyze the patterns of coupled CO_2 sequestration and oil production in micropores under the original reservoir conditions during CO_2 flooding. The CO_2 dissolution sequestration in the residual mixed fluids (residual oil and water) in reservoirs after CO_2 displacement is calculated by the CO_2 dissolution sequestration coefficient (E_s) with the CO_2 dissolution ability data by a series of experiments of CO_2 dissolution. The impact of residual water saturation within cores on the CO_2-induced changes in minerals, pore structures, and wettability of cores is characterized by SEM, XRD, and contact angle measurement of core slices before and after CO_2—water—oil—rock interaction. The microscopic oil production and CO_2 sequestration are analyzed by the sensitivity analysis of the CO_2 injection pressure, residual water saturation, and the CO_2—water—oil—rock interaction during CO_2 displacement.

2. Theoretical basis

2.1. Coupling mechanism of CO_2 displacement and sequestration

During CO_2 injection into reservoirs, CO_2 initially occupies the partial pore spaces within reservoirs due to the production of fluids (water and oil) and is retained in the pores through the mechanisms of CO_2 structural sequestration and residual sequestration. As the duration of contact time between CO_2 and residual fluids in the formation increases, the CO_2 trapped within pore spaces dissolves in the residual oil and water, which is formed as CO_2 dissolution sequestration. Finally, CO_2 dissolved in the residual formation water reacts with the rock for millions of years, resulting in permanent mineral deposits (referred to as CO_2 mineral sequestration) (Zhao et al., 2015; Zhang et al., 2019).

By changing the technical parameters of CO_2 flooding, the oil recovery and CO_2 sequestration in reservoirs are all improved simultaneously (He et al., 2016). The patterns of CO_2-enhanced oil recovery and sequestration in micropores of reservoirs can be analyzed by the changes in the area of NMR spectra and the NMR

image. The CO_2 dissolution sequestration in residual fluids (oil and water) in reservoirs after CO_2 flooding is mainly influenced by the residual oil and water saturation and the total volume of the residual mixed fluids. In this study, CO_2 dissolution patterns in the residual fluids of cores are analyzed with the CO_2 dissolution sequestration coefficient (E_s) proposed by us in Eq. (1) and the CO_2 dissolution experiment under various reservoir temperature and pressure conditions. The evolutions of minerals, pore structures, and wettability of cores and their impact on CO_2-EOR and ECS during the CO_2 injection process were also studied through CO_2–water–oil–rock interaction experiments, as well as SEM, XRD, contact angle analysis, and NMR T_2 spectrum analysis.

$$E_s = S_{or}R_o + S_{wr}R_w \tag{1}$$

where E_s is the CO_2 dissolution sequestration coefficient; S_{or} is the residual oil saturation; S_{wr} is the residual water saturation; R_o is the solubility of CO_2 in oil, kg/kg; R_w is the solubility of CO_2 in formation water, kg/kg.

2.2. Analytical methods of CO_2 displacement and sequestration in micropores

The analytical method of CO_2-EOR and ECS in micropores with NMR T_2 spectrum is demonstrated in Fig. 1, where the abscissa represents the T_2 relaxation time of the oil- or water-saturated core and the ordinate represents the NMR signal intensity of hydrogen-containing fluids in different scales of pores. The T_2 relaxation time primarily consists of the bulk volume relaxation time T_{2b}, surface relaxation time T_{2s}, and diffusion relaxation time T_{2d}, as detailed in Eq. (2) (Yang et al., 2013; Zhang et al., 2024a).

$$\frac{1}{T_2} = \frac{1}{T_{2b}} + \frac{1}{T_{2s}} + \frac{1}{T_{2d}} \tag{2}$$

where T_2 is the transverse relaxation time, ms; T_{2b} is the bulk volume relaxation time, ms; T_{2s} is the surface relaxation time, ms; and T_{2d} is the diffusion relaxation time, ms.

For the fluid flow in porous media, the components T_{2b} and T_{2d} are disregarded when the magnetic field exhibits a homogeneous gradient throughout the medium (Wang et al., 2018; Fan et al., 2022). Therefore, the T_2 relaxation time primarily relies on the surface relaxation time T_{2s}, which can be characterized using Eq. (3).

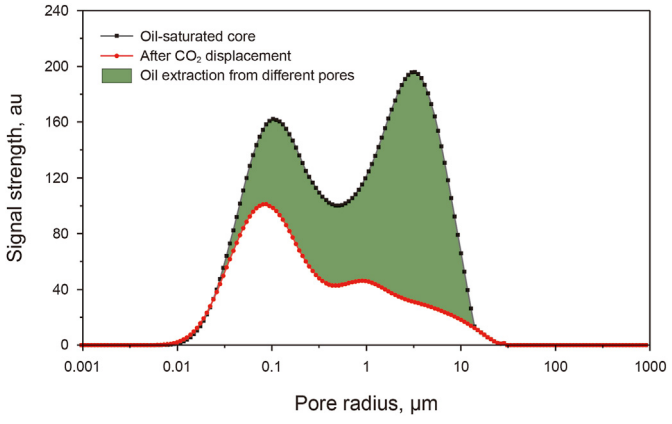


Fig. 1. Typical NMR T_2 spectra of the core with oil-saturated and after CO_2 displacement.

$$\frac{1}{T_2} = \frac{1}{T_{2s}} = \rho_2\left(\frac{S}{V}\right) \tag{3}$$

where ρ_2 is the surface relaxation coefficient, μm/ms; S is the pore surface area of rock, μm^2; V is the pore volume, μm^3.

Additionally, the ratio S/V can be interpreted as a dimensionless ratio of the pore shape factor F_s and pore radius r such as Eq. (4).

$$T_2 = T_{2s} = \frac{1}{\rho_2 F_s} r \tag{4}$$

where r is the pore radius, μm; F_s is the pore shape factor.

Conventionally, the surface relaxation coefficient ρ_2 and the shape factor F_s are presumed to remain constant based on the research by Lai et al. (2018). Therefore, Eq. (4) can be written as the conversion of Eq. (5) (Saidian and Prasad, 2015). According to Eq. (5), the greater the pore radius, the longer the T_2 relaxation time of the core will be, while a smaller pore radius in the core will result in a shorter T_2 relaxation time. In this equation, the conversion coefficient C is mainly related to the reservoir properties such as the heterogeneity of pores, the size of pores, etc.

$$T_2 = C \times r \tag{5}$$

where C is conversion coefficient between T_2 relaxation time and pore radius, ms/μm.

In this experiment, the coefficient C in Eq. (5) is determined by referring to the methods proposed by Zhao et al. (2019). Firstly, the T_2 spectrum of the oil-saturated Core No. 2 is tested and the average T_2 relaxation time (T_{2av}) is calculated with Eq. (6).

$$T_{2av} = \exp\frac{\sum \ln(T_{2i}\varphi_i)}{\sum \varphi_i} \tag{6}$$

where T_{2av} is the average T_2 relaxation time, ms; T_{2i} is the relaxation time of the i-th pore, ms; φ_i is the nuclear magnetic signal intensity at a relaxation time of T_{2i}.

Afterward, the core is washed with toluene and dried in an oven for 24 h. After that, the average pore radius r_a of the dried core is obtained with the mercury intrusion experiment. The average relaxation time T_{2av} and the average pore radius r_a of the core are substituted into Eq. (5) for the calculation of C. Due to the similar physical properties of the two cores drilled from the same reservoir interval, the same C is used for the conversion of T_2 relaxation time to pore radius r of the two cores.

To better understand the CO_2 sequestration capacity in reservoirs during CO_2 flooding, we have introduced the concept of the CO_2 sequestration ratio in reservoir pores, as shown in Eq. (7).

$$E_c = \frac{V_{sq}}{V_p} \times 100\% \tag{7}$$

where V_{sq} is the CO_2 sequestration volume in pores of cores after CO_2 displacement, m^3; V_p is the total pore volume of cores, m^3.

Based on the principle of mass conservation in reservoirs, if the pressure and temperature of the reservoir remain constant (70 °C, 14.3 MPa), and there is no leakage of CO_2 during the injection process. The higher the oil and water recovery achieved from reservoirs through CO_2 displacement, the greater the amount of CO_2 retained within the reservoir pores after CO_2 injection. Therefore, the oil recovery and CO_2 sequestration ratio in cores can be calculated using the same NMR spectra area methodology, as described in Eq. (8).

$$E_{ci} = E_c = \frac{S_{i1} - S_{i2}}{S_{i1}} \times 100\% \quad (8)$$

where E_{ci} is the liquid recovery calculated by the NMR peak area method, %; E_c is the CO_2 sequestration ratio in the cores, %; S_{i1} is the area of NMR spectrum of the oil-saturated core; S_{i2} is the area of NMR spectrum of the oil-saturated core after CO_2 displacement.

The NMR signal intensity in the T_2 spectrum is mainly related to the content of fluids with H^1 protons. For example, the higher amount of oil in the pores means a higher NMR signal intensity for the tested core. The injected CO_2 does not have the NMR signal. Therefore, the change of the NMR T_2 spectra of cores tested at various time intervals can reveal the oil extraction degree and CO_2 sequestration within distinct micropores during CO_2 flooding. Furthermore, the NMR image's brightness variations offer insights for the analysis of the change of the oil content and CO_2 storage in distinct regions within the core. The brighter NMR image of the tested core means that the residual oil or water content in a certain area of the core is higher and the CO_2 stored in this area is less.

3. Experiment design

Based on the slim tube experiments, the MMP between CO_2 and formation oil for the target oilfield is 27.2 MPa at 70 °C. Before CO_2 displacement experiments, all core samples were thoroughly washed with toluene to eliminate residual oil. Subsequently, the cleaned cores were placed in an oven and heated to 100 °C for 24 h. The impact of CO_2 injection pressure, residual water saturation of reservoirs, and CO_2–water–oil–rock reaction on CO_2-EOR and ECS were studied by CO_2 displacement and CO_2–water–oil–rock interaction experiments. The CO_2 dissolution sequestration in different proportions of oil–water mixtures in reservoirs was also analyzed with the help of the CO_2 dissolution experiments.

3.1. Materials and equipment

The experimental cores and slices (Figs. 2 and 3) used for the experiments were obtained from well X6 within the CY oilfield with a burial depth of 1390 m. The temperature and pressure at the target layer are 70 °C and 14.3 MPa, respectively. The physical properties and mineral compositions of the two experimental core samples employed are listed in Tables 1 and 2. The density and viscosity of crude oil are 0.89 g/cm^3 and 6.8 cP at room temperature, respectively. The formation water synthesized in the laboratory is $NaHCO_3$ type with a salinity of 8515 mg/L. A mass fraction of 7% manganese tetrachloride ($MnCl_4$) is added to the synthesized water to inhibit NMR signals when necessary. The water density is 1.13 g/cm^3 at room temperature. The purity of CO_2 is 99.99%. Fluoride solution (FC-40) is utilized to exert confining pressure and temperature to the core samples within a non-magnetic core holder.



Fig. 2. Appearance of experimental cores.

An NMR scanner, specifically the MesoMR12-060H-I with a magnetic field strength of 0.5 T, was employed to analyze the distribution of oil and CO_2 within micropores. Additionally, a scanning electron microscope (SEM) and an X-ray diffraction meter (XRD) were utilized to characterize the mineral morphology and compositions of the cores after the CO_2–water–rock reaction. A CO_2 booster pump (TES-92) was used for CO_2 pressurization and injection. The wettability of the cores was tested using a contact angle tester (SZ100-JC2000C). In the process of the in-situ NMR tests, a heat-shrink tube without NMR signals was used to seal the cores and isolate the fluoride solution from the core samples. The non-magnetic core holder was used to hold the sealed core and tested the NMR signal at different CO_2 injection time nodes.

3.2. Experimental process

Fig. 4 shows the flowchart of the experimental procedures in this study, including CO_2 dissolution, CO_2 displacement, and the CO_2–water–oil–rock interaction experiments. The CO_2 dissolution experiments were designed to study the CO_2 dissolution capacity in the residual fluids within the micropores of cores after CO_2 injection. The effects of CO_2-EOR and ECS in the micropores of reservoirs are primarily affected by the CO_2 injection pressure and the residual water saturation. The CO_2 injection pressure affects the mass transfer and IFT between CO_2 and formation oil, leading to different CO_2 displacement and sequestration effects within the micro pores. The variations of residual water saturation within reservoirs result in different reaction rates and degrees between CO_2, water, and rock. This leads to distinct changes in the pore volume increment and surface wettability improvement of the reservoir rock, ultimately altering the CO_2-EOR and ECS effects. Therefore, in our studies, CO_2 displacements combined with the in-situ NMR testing are conducted to study the microscopic coupled effect of CO_2-EOR and ECS in reservoir pores. Furthermore, the CO_2–water–oil–rock interaction experiments are designed to analyze the changes in minerals, pore structures, and wettability before and after CO_2 injection, which also help reveal the mechanism of EOR and ECS. The following sections show a detailed description of the experimental procedures.

3.2.1. CO_2 dissolution experiment

To investigate the CO_2 dissolution sequestration in the residual mixed formation fluids after CO_2 displacement under various temperature and pressure conditions, we conducted a CO_2 dissolution experiment (see Table 3). A schematic representation of the device is shown in Fig. 5 and the process covers the following steps: (1) First, 60 mL of formation fluid was poured into the reactor. (2) After the reactor is sealed, the fluid inside the reactor is heated to the designed experimental temperature by using an electric heating jacket. After the temperature is stabilized for 20 min, the compressed CO_2 is injected into the reactor to attain experimental pressures. (3) The CO_2-inlet valves on the cylinder are closed for the CO_2 dissolution experiment. (4) The magnetic stirrer is turned on to stir the mixtures of fluids and CO_2 inside the cylinder, allowing CO_2 to quickly dissolve in oil or water. (5) After 2 h, the bottom mixture of CO_2-liquid for a single phase is discharged from the valve at the bottom of the reactor. Meanwhile, CO_2 is injected from the top of

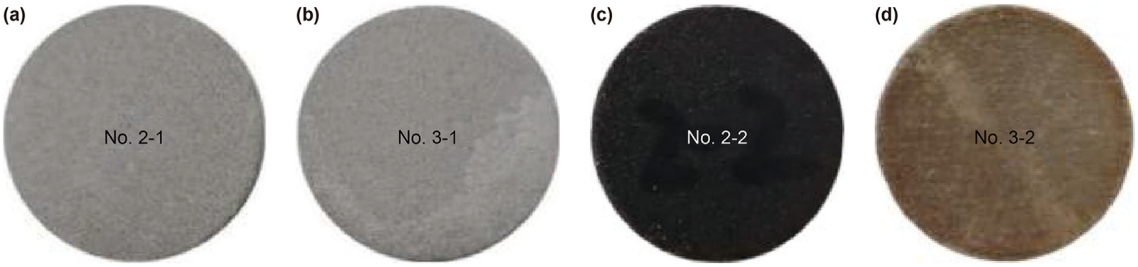


Fig. 3. Core slices for CO_2–water–oil–rock reaction experiment: (**a**, **b**) core slices after drying and oil washing, (**c**) oil-saturated core slice only with bound water, (**d**) core slice with residual water saturation of 0.5.

Table 1
Physical parameters of the experimental cores.

Core ID	Diameter, cm	Length, cm	Permeability, mD	Porosity, %
No. 2	2.5	10	45.38	17.8
No. 3	2.5	7	35.09	15.6

the reactor to maintain a constant experimental pressure inside the reactor, reducing experimental errors caused by pressure changes inside the reactor. (6) The CO_2-oil/water mixtures discharged from the reactor are poured into the gas–liquid separator to facilitate the separation of CO_2 and liquids. The solubility of CO_2 in oil or water is also determined by the results of the gas–liquid separation. (7) Based on the residual oil and water saturation of cores after the CO_2 displacement in Section 3.2.2 and the CO_2 dissolution sequestration coefficient Eq. (1), the CO_2 dissolution sequestration capacity in the residual fluids of reservoirs is analyzed after CO_2 displacement.

3.2.2. CO_2 displacement experiment

The scenarios of CO_2 displacement experiments with core samples (oil-saturated and $S_{wr} = 0.5$) are listed in Table 4. The experiment process of CO_2 displacement with the in-situ NMR testing can refer to Zhang et al. (2024a, 2024b), covering the following steps: (1) Cores No. 2 and No. 3 are washed with toluene, and then dried at a constant temperature oven with 100 °C for 24 h. (2) The two cores are initially saturated with water and oil through

Table 2
Mineral composition analysis of experimental cores.

Core ID	Mineral composition, %					
	Illite	Potassium feldspar	Sodium feldspar	Quartz	Kaolinite	Calcite
No. 2	2.0	13.8	46.9	25.6	6.6	5.1
No. 3	2.3	12.9	44.6	26.5	7.8	5.9

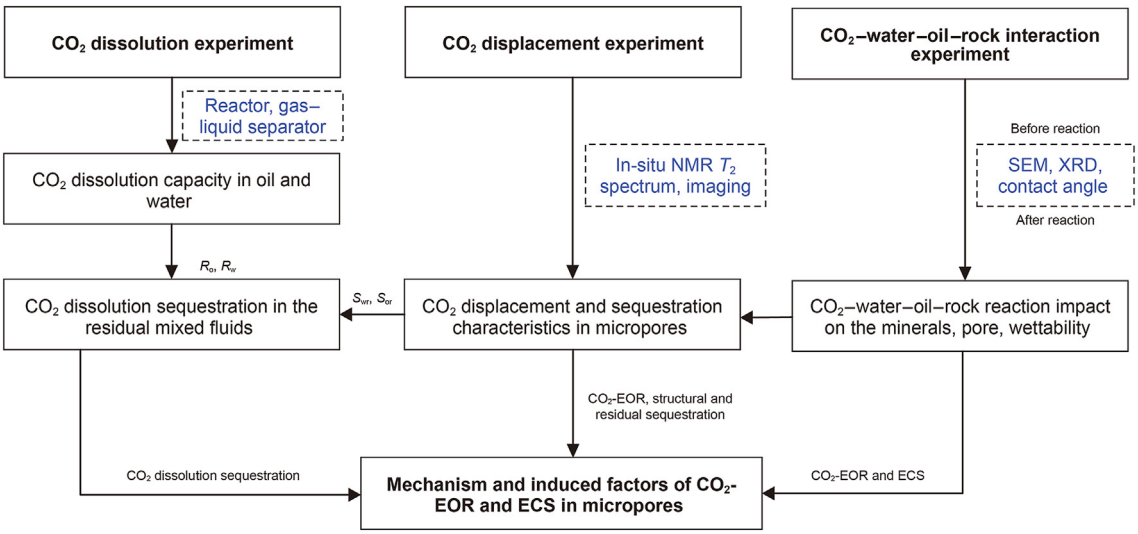


Fig. 4. Flowchart of the experimental procedures of CO_2 displacement and sequestration.

Table 3
Experiment scenarios of CO_2 dissolution in formation fluids.

Fluid type	Pressure, MPa	Temperature, °C	Reaction duration, h	Solubility of CO_2 in oil and water, m^3/m^3
Oil/water	3, 5, 7, 10, 15, 20, 25, 30	30, 50, 70, 90, 100, 110	2	R_o, R_w

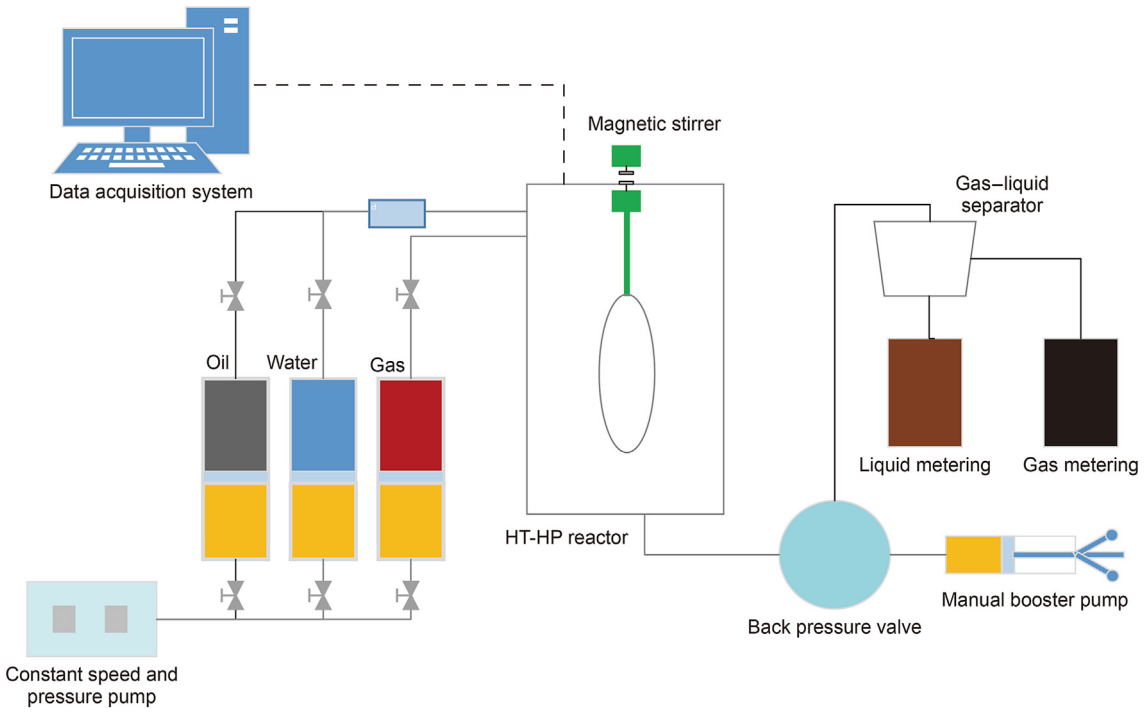


Fig. 5. Experimental process of CO_2 dissolution in oil or water.

Table 4
Experiment scenarios of CO_2 displacement.

Core ID	Sample state	Pressure, MPa	Temperature, °C	Testing time nodes, min	NMR data
No. 2	Oil-saturated/S_{wr} = 0.5	10/15	70	30/60/120	T_2 spectra, image
No. 3	Oil-saturated/S_{wr} = 0.5	10/15	70	30/60/120	T_2 spectra, image

continuous oil displacement. (3) The oil-saturated cores aree placed in the non-magnetic core holder. After the experimental temperature are heated up to 70 °C, the NMR T_2 spectra and images of the cores are tested with the CPMG and HSE sequences with the sequence parameters (CPMG: main frequency, 12 MHz; sampling frequency, 200 kHz; waiting time, 6000 ms, echo time, 0.5 ms; number of echoes, 3000; HSE: phase encoding duration, 1 ms; echo position, 10 %; TE, 4.3 ms; averages, 4). (4) CO_2 displacement experiments are conducted at the pressure of 10 and 15 MPa, respectively. The NMR T_2 spectra and images are tested every 30 min, and the oil recovery is also calculated by the peak area methodology of NMR spectra described in Eq. (8). The T_2 spectra and images at different CO_2 flooding time nodes are compared to analyze the oil production and CO_2 sequestration. (5) The cores after the first CO_2 displacement and CO_2–water–oil–rock interaction are washed to remove the residual oil. (6) After that the dried cores are saturated with the manganese water, and the water-saturated cores are displaced through continuous oil injection. When the produced water in the tube is half of the saturated water in the cores, the water saturation (S_{wr}) was 0.5. (7) Afterward, CO_2 displacement experiments are repeatedly conducted to analyze the impact of CO_2–water–oil–rock on CO_2-EOR and ECS.

3.2.3. CO_2–water–oil–rock interaction experiment

The CO_2–water–oil–rock experiment is conducted to analyze the impact of the interaction on CO_2 EOR and ECS. The experimental scenarios are listed in Table 5, and a schematic of the workflow can refer to Zhang et al. (2024b). The experiment steps are as follows: (1) After the CO_2 displacement experiment in Section 3.2.2, the cores No. 2 and No. 3 were washed and dried in a constant temperature oven. (2) Two pairs of slices with a thickness of 0.5 cm, cut from the dried cores, are noted as No. 2-1, No. 2-2, No. 3-1, and No. 3-2, respectively. (3) The initial contact angles of the water phase as well as the mineral morphology of core slices (No. 2-2 and No. 3-2) are measured using the contact angle tester and SEM. The testing process of contact angle mainly refers to the test method for wetting angle of rocks by Yang et al. (2008). The testing process of SEM involves polishing the surface of core slices and spraying a very thin layer (10 nm thick) of gold on the surface of the polished rock samples to enhance conductivity, therefore improving the scanning effect. After scanning the core slices with an accelerated voltage range of 10–15 kV, SEM images are obtained. (4) Half of the core slices (No. 2-1 and No. 3-1) are crushed to powder below 200 mesh, and the continuous XRD scanning analysis with testing parameters (The current and voltage of the tube are 150 mA and 40 kV; scanning range, 5°–64°; scanning step, 0.02°; scanning speed, 2°/min) is performed to determine the mineral composition of the cores. (5) The core No. 2 and core slice No. 2-2 are saturated with manganese water and oil sequentially, and the core slice No. 3-2 is made with a water saturation of 0.5. (6) After 600 mL of formation water is injected into the reactor, the oil-saturated core No. 2 and the slices No. 2-2, and No. 3-2 are put into the reactor. (7) After the formation water inside the reactor is heated to 70 °C, the CO_2 is pressurized to 15 MPa and injected into the reactor. The reaction of CO_2–water–oil–rock is last for 16 days. (8) All the samples after the reaction are washed and dried, and the mineral morphology,

Table 5
Experiment scenarios of CO_2–water–oil–rock interaction.

Core ID	Sample state	Pressure, MPa	Temperature, °C	Reaction duration, day
No. 2 and slice	Oil-saturated	15	70	16
No. 3 and slice	$S_{wr} = 0.5$	15	70	16

compositions, and contact angle of the water phase of the dried core slices (No. 2-2 and No. 3-2) are measured. (9) The core No. 2 after the reaction experiment is saturated with water and oil. (10) The CO_2 displacement experiments with the repeated oil-saturated core No. 2 are conducted repeatedly to analyze the impact of the interaction on the oil recovery and CO_2 sequestration.

4. Experimental results

4.1. CO_2 dissolution capacity in reservoirs

After the CO_2-EOR process in a reservoir, the trapped CO_2 in the pores comes into contact with and dissolves into the residual fluids. Due to the different solubility of CO_2 in formation oil and water, the dissolution sequestration of CO_2 in the residual fluids will vary under different saturation conditions of residual oil and water. The results of CO_2 dissolution ability in the formation water and oil are shown in Fig. 6. The CO_2 solubility in oil and water increases with the pressure increase or the temperature decrease. However, the solubility of CO_2 in oil is stronger than in formation water. By conducting CO_2 dissolution experiments in oil and brine, similar CO_2 dissolution patterns in oil and water at different temperatures and pressures were found by Steel et al. (2016) and Davarpanah and Mirshekari (2020). Furthermore, as the pressure rises from 5 to 7 MPa, the solubility of CO_2 in water rapidly increases. However, the increased amplitude of CO_2 solubility in water slows down when the pressure increases from 7 to 30 MPa because the CO_2 solubility in water is close to the maximum CO_2 solubility. On the contrary, the CO_2 solubility in the oil is strengthened after 7 MPa, since the contact pressure rise accelerates the mass transfer between CO_2 and oil, leading to a quicker CO_2 dissolution in oil phases. However, compared with the impact of temperature on the solubility of CO_2 in water at low-pressure conditions (3 MPa), its effect on the solubility of CO_2 in oil is not significant under similar low-pressure conditions.

To analyze the CO_2 dissolution sequestration in the residual fluids in cores after CO_2 displacement, core No. 2 in Section 3.2.2 is taken as an example. The residual oil saturation (S_{or}) of the oil-saturated core after CO_2 displacement (in Section 4.2) is 0.488 and the residual water saturation (S_{wr}) is only 0.01. For the core with $S_{wr} = 0.5$, the residual oil saturation and residual water saturation are 0.288 and 0.09, respectively. By the calculation with Eq. (1), the CO_2 dissolution sequestration coefficient (E_s) within the mixed residual fluids is shown in Fig. 7. The E_s is higher within residual fluids for the oil-saturated core after CO_2 displacement because of the higher residual oil saturation for the core after CO_2 injection. However, the CO_2 dissolution sequestration coefficient is lower at the real reservoir temperature and pressure (70 °C, 14.3 MPa). Therefore, during the CO_2-EOR process, the reduced residual oil saturation in reservoirs reduces the amount of CO_2 dissolution sequestration but induces little impact on the whole CO_2 sequestration amount within reservoirs.

4.2. Oil extraction and CO_2 sequestration in micropores

The oil extraction and CO_2 sequestration in micropores of cores (oil-saturated and $S_{wr} = 0.5$) during CO_2 displacement are shown in Fig. 8. The pore heterogeneity of the two experimental cores is different, which leads to the differential fluids distribution in the pores of cores and the different NMR signal intensity in different pores. The NMR signal in the region of large pores of oil-saturated core No. 3 with low porosity and permeability was higher than that of core No. 2, while the NMR signal of the small pore region for core No. 3 was lower than that for core No. 2. During the first 30 min of the CO_2 displacement process, oil is extracted from both large and small pores, but the produced oil is higher from large pores. During the 30–60 min of CO_2 immiscible flooding, the residual oil is primarily recovered from larger pores, whereas the quantity of oil extracted from smaller pores is little. However, the produced amount of residual oil in small pores is increased during 60–120 min of CO_2 immiscible flooding due to the lower residual oil saturation in large pores in this displacement stage. The oil in cores No. 2 and No. 3 is mainly produced from the pores exceeding the pore radius of 0.04 and 0.02 μm with oil recovery of 51.2% and 52.8%, respectively. Since the water present in the oil-saturated cores is only bound water, the oil recovery and liquid recovery are similar. Therefore, the CO_2 sequestration ratio in the cores is also approximately the same as the oil recovery.

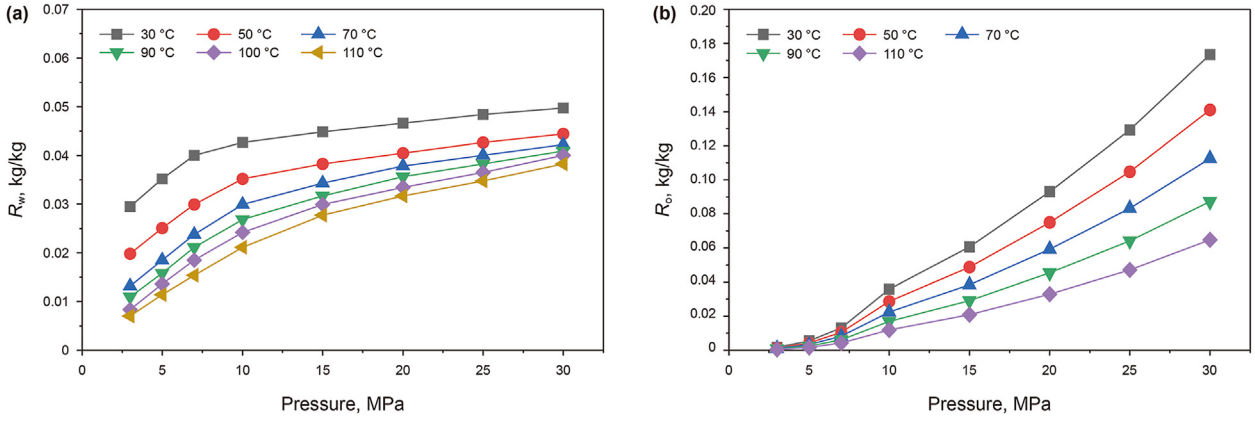


Fig. 6. CO_2 solubility in formation water (**a**) and oil (**b**).

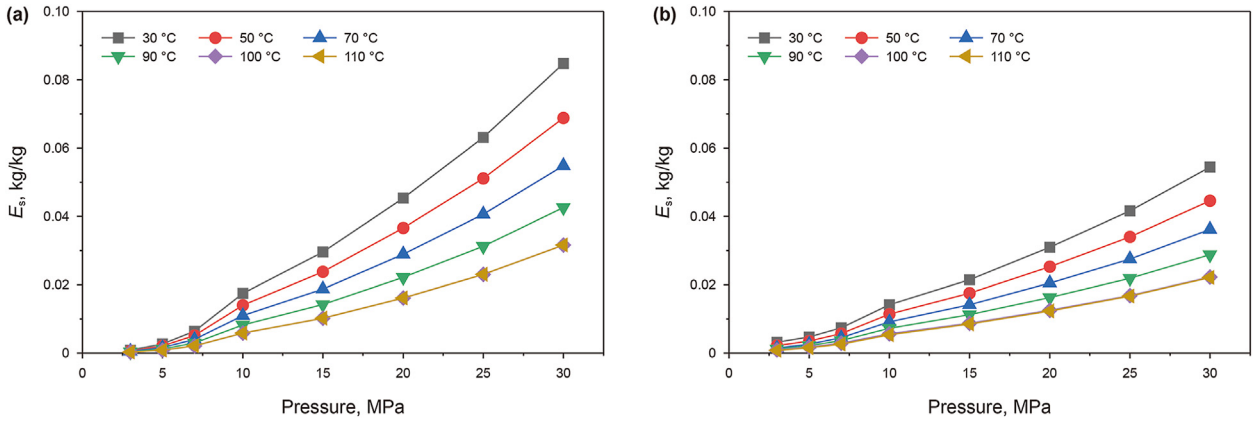


Fig. 7. CO_2 dissolution sequestration coefficient in residual fluids in core No. 2. (**a**) $S_{or} = 0.488$, $S_{wr} = 0.01$; (**b**) $S_{or} = 0.288$, $S_{wr} = 0.09$.

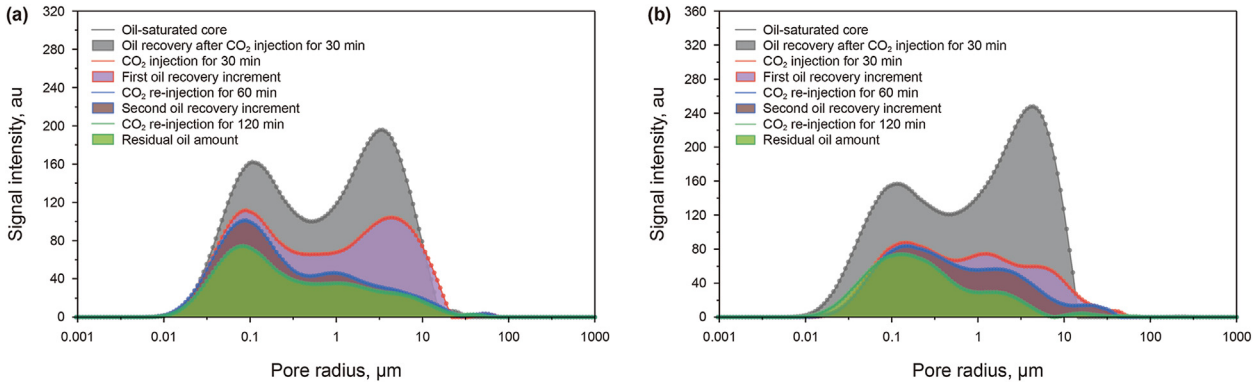


Fig. 8. Oil extraction and CO_2 sequestration in micropores of cores after different CO_2 injection times: (**a**) oil-saturated core No. 2; (**b**) oil-saturated core No. 3.

Compared with the oil extraction and CO_2 storage in micropores of oil-saturated cores, the oil recovery and CO_2 sequestration in micropores of cores ($S_{wr} = 0.5$) are shown in Fig. 9. The oil is uniformly extracted from the small and large pores of cores within the first 60 min of CO_2 immiscible flooding. However, during the 60–120 min of CO_2 immiscible flooding, the incremental oil recovery remains minimal due to gas breakthrough from the outlet of cores. Moreover, the pore size threshold for oil production in the cores ($S_{wr} = 0.5$) is significantly higher, ranging from 0.05 to 0.06 μm, compared with that of the oil-saturated cores. In theory, the reduction in reservoir water saturation can promote the entering of CO_2 into smaller pores, thereby improving the effect of CO_2 displacement and storage. However, we found the liquid recovery and oil recovery of cores No. 2 and No. 3 ($S_{wr} = 0.5$) are higher with 62.2% and 53%, 65.8% and 57%, respectively. According to the patterns of matter conservation in the pore space of cores during the CO_2 displacement process, the more fluid is extracted from the core, the more CO_2 is stored in the pore spaces of the core, which indicates the CO_2 sequestration ratio in reservoirs with a certain water saturation is better. Zhou et al. (2024) also confirmed that CO_2 injection into the reservoir with a water saturation of 0.513 can achieve 72% pore volume of CO_2 sequestration, and the oil recovery is greatly improved due to the replacement effect of fluids by CO_2 injection in the reservoir pores. When CO_2 is injected into the oil-saturated cores, although the pore size threshold of produced oil is lower, the CO_2 breakthrough in cores is also earlier due

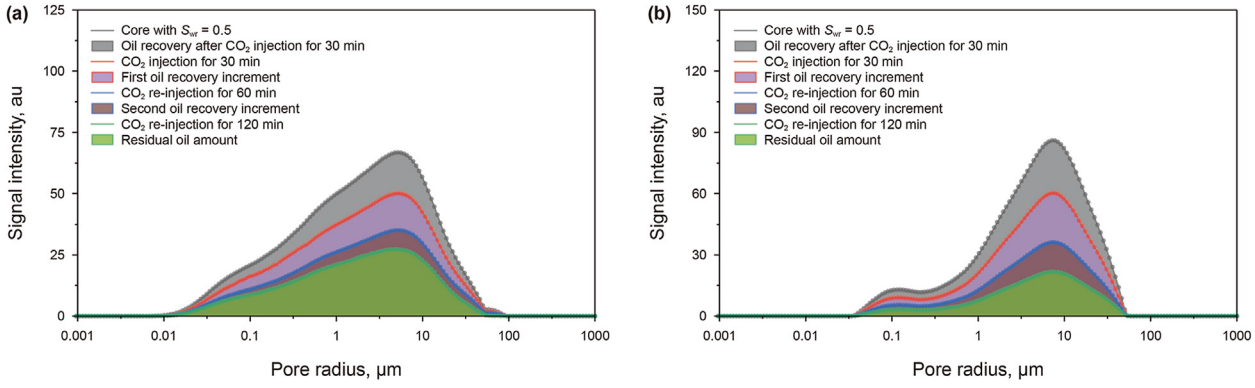


Fig. 9. Oil extraction and CO_2 sequestration in micropores of cores after different CO_2 injection times: (**a**) core No. 2 with $S_{wr} = 0.5$; (**b**) core No. 3 with $S_{wr} = 0.5$.

to the high viscosity ratio between CO_2 and oil, which results in the low oil recovery. Moreover, a certain stage of water injection before CO_2 injection also leads to a certain amount of oil recovery, resulting in a higher final oil recovery for reservoirs than that by direct CO_2 injection. In addition, the degree of CO_2–water–rock reaction is higher in cores with a water saturation of 0.5 than that in oil-saturated cores after CO_2 injection, resulting in better hydrophilicity improvement on the pore surface of cores ($S_{wr} = 0.5$). The enhancement of rock hydrophilicity is beneficial for CO_2 injection to remove adhered oil on the surface of pores and also enhances the imbibition ability for displacing oil. CO_2 sequestration within reservoirs after CO_2 injection is mainly achieved by replacing the mixed fluids in reservoir pores. Compared to the oil content in the small pores of cores with a water saturation of 0.5, the oil content in the small pores of cores with saturated oil is higher, which also leads to low oil recovery for oil-saturated cores. Therefore, for cores with a water saturation of 0.5, the fluid recovery is higher after CO_2 displacement, and the effect of CO_2 sequestration is also better.

The visualized oil production and CO_2 sequestration in cores No. 2 and No. 3 during immiscible CO_2 displacement is analyzed with the brightness change of the NMR images (Fig. 10). For the oil-saturated cores, oil is produced gradually from cores with the extension of CO_2 immiscible displacement time. After 120 min of CO_2 displacement, the NMR images of cores have darkened due to the CO_2 without a nuclear magnetic signal occupying the pore spaces. However, the images of the injection end of oil-saturated cores are darker than that of the outlet end of cores because of the greater pore volume number of CO_2 injection, which indicates the CO_2-EOR effect in the near well region is better and more CO_2 is retained near the wellbore. For cores with $S_{wr} = 0.5$, due to conducting a certain stage of manganese water flooding, the brightness of the NMR images of cores is lower than that of the oil-saturated cores before CO_2 flooding. After 120 min of continuous CO_2 injection, the brightness of the NMR images of the cores ($S_{wr} = 0.5$) is lower than that tested of the oil-saturated cores after CO_2 flooding, which reveals that the oil extraction effect of reservoirs with CO_2 immiscible displacement after a stage of water flooding is better.

On the other hand, the lower brightness of NMR images of tested cores after CO_2 displacement means a higher liquid or oil recovery. According to the conservation law of matter in porous media, the pore space of the produced oil and water is occupied by the injected CO_2 in reservoirs. Therefore, the CO_2 sequestration ratio in cores with $S_{wr} = 0.5$ is also better than that in oil-saturated cores.

4.3. CO_2-induced changes in mineral and pore structure

The formation oil adhered to the rock surfaces of pores isolates the contact of rock with formation water, which will hinder the CO_2–water–rock reaction. This inhibition effect will vary with the water saturation of reservoirs. The mineral changes within the oil-saturated core No. 2 before and after the CO_2–water–oil–rock are shown in Fig. 11. The dissolved minerals are mainly calcite, while the formed minerals predominantly consist of kaolinite on the surface of the rock during CO_2 flooding, as detailed in Eqs. (9)–(13). The plane porosity of the core slices increases from 17.1% to 22.3%, accompanied by an expansion in the pore size range from 0.3–130 μm to 0.7–135 μm after the CO_2–water–oil–rock reaction. Additionally, these results suggest that the dissolution of the minerals leads to an increase in the porosity of rock slices, which enhances the CO_2 sequestration capacity within the reservoir.

As a comparison, the mineral changes of core No. 3 ($S_{wr} = 0.5$) before and after the reaction are shown in Fig. 12. It has been observed that the dissolution of minerals is more intense, resulting in the formation of a larger corrosion pit of calcite on the surface of the rock after the CO_2–water–oil–rock reaction. An irregular zigzag shape of the dissolution boundary is also observed for feldspar minerals. Additionally, notable elevations in the plane porosity of the core slices are observed, ranging from 15.3% to 23.4%. An expansion in the range of pore sizes, from 0.3–67 μm to 0.3–174 μm, has been also observed after the CO_2–water–oil–rock reaction. This indicates that an increase in the water saturation will enhance the reaction degree of CO_2–water–rock, leading to a greater increment in pore volume and thereby improving the CO_2 storage effect in reservoirs.

$$CO_2 + H_2O \leftrightarrow H_2CO_3 \leftrightarrow H^+ + HCO_3^- \tag{9}$$

$$\text{Calcite: } CaCO_3 + Ma^{2+} + Fe^{2+} + HCO_3^- \leftrightarrow CaMg_{0.3}Fe_{0.7}(CO_3)_2 \tag{10}$$

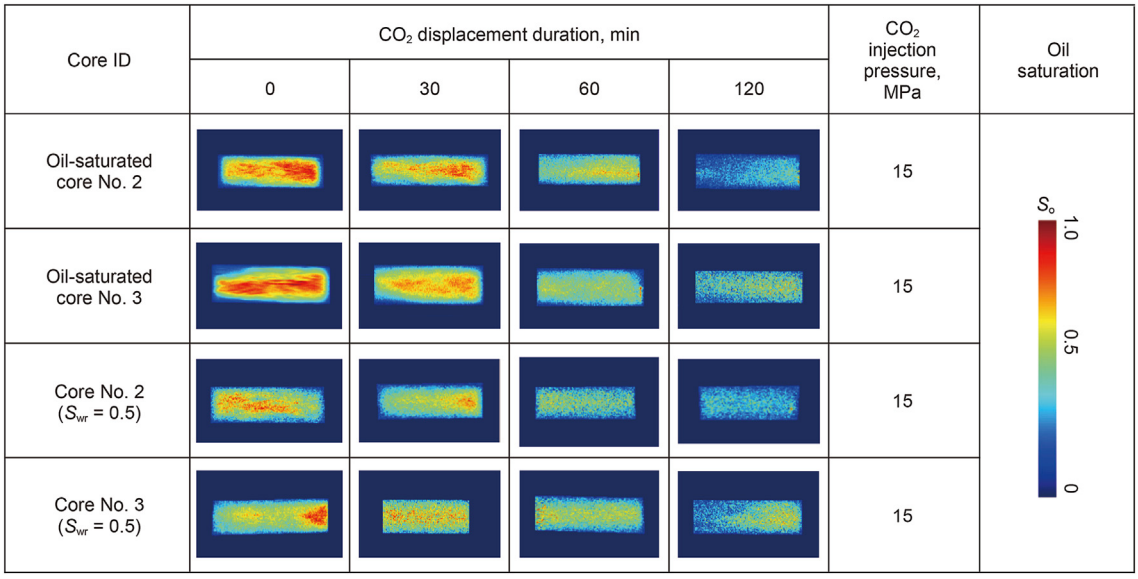


Fig. 10. NMR images of the cores with different residual water saturations at different time nodes of CO_2 displacement.

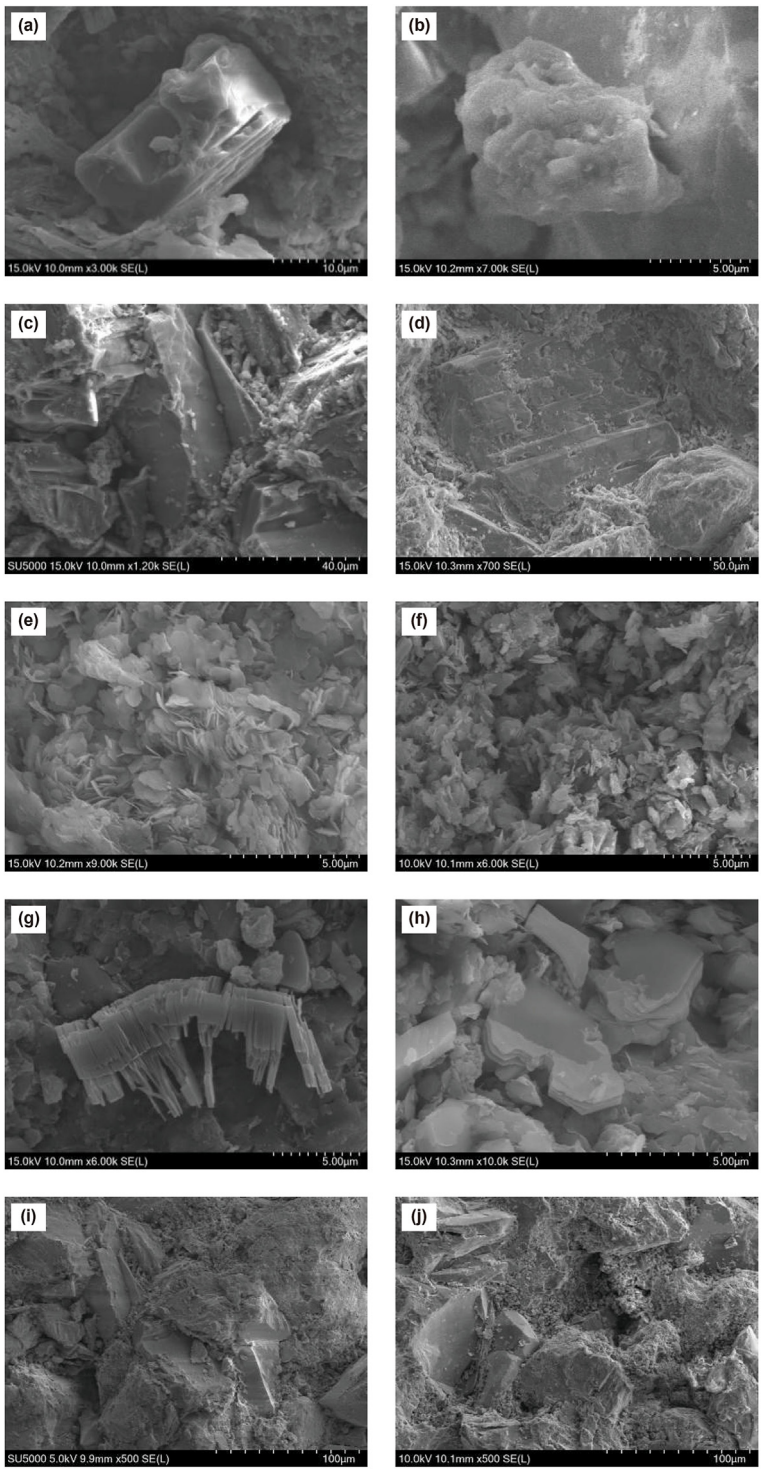


Fig. 11. Morphology change of minerals before and after CO_2–water–oil–rock interaction for the oil-saturated core No. 2 slice (reaction time, 16 days): (**a**, **c**, **e**, **g**) calcite, feldspar, chlorite, kaolinite before reaction; (**b**, **d**, **f**, **h**) calcite, feldspar, chlorite, kaolinite after reaction; (**i**, **j**) pore structures before and after reaction.

$$\text{K-feldspar}: 2KAlSi_3O_8 + 2H^+ \leftrightarrow Al_2Si_2O_5(OH)_4 + 2K^+ + 4H_4SiO_4 \quad (11)$$

$$\text{Na-feldspar}: 2NaAlSi_3O_8 + 3H_2O + 2CO_2 \leftrightarrow Al_2Si_2O_5(OH)_4 + 2Na^+ + 2HCO_3^- + 4SiO_2 \quad (12)$$

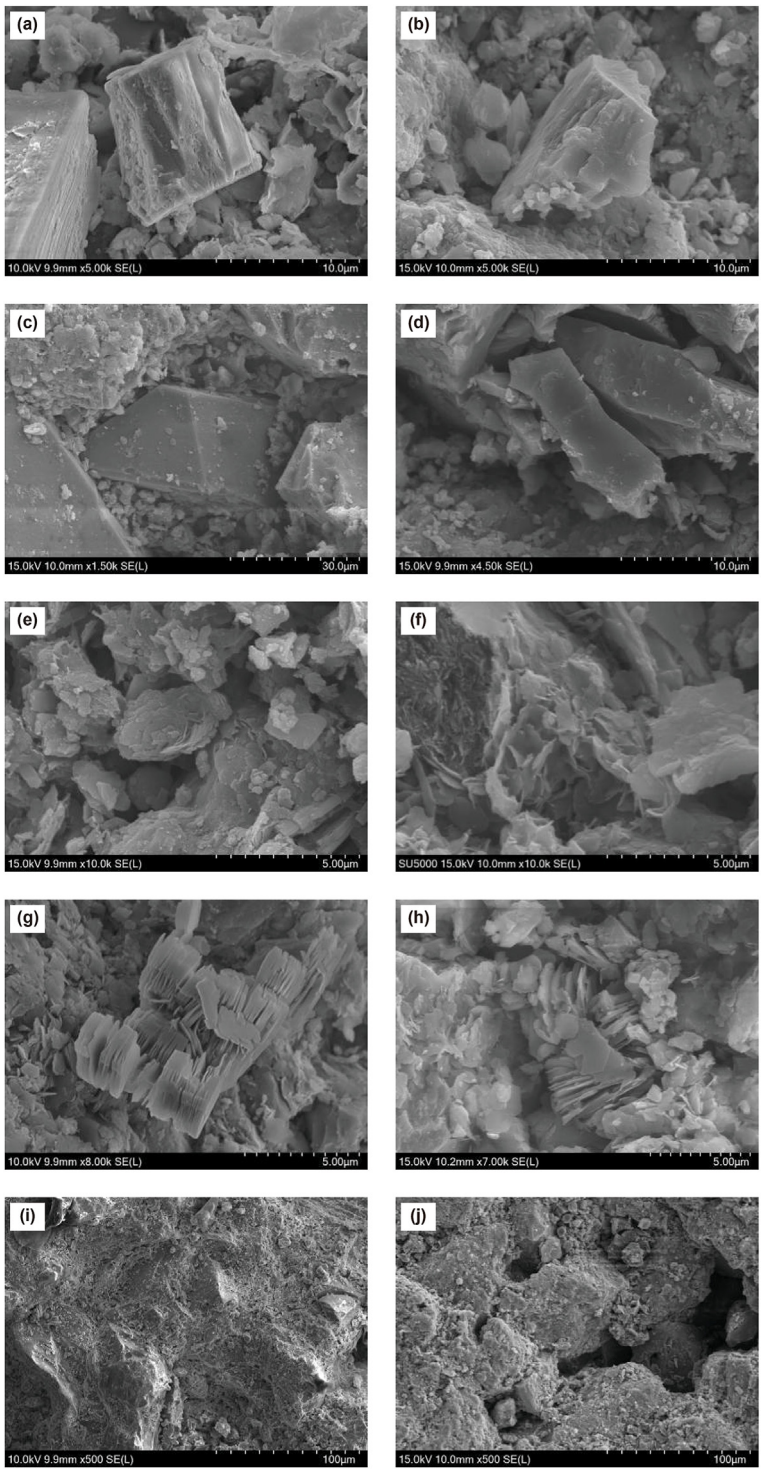


Fig. 12. Minerals morphology change before and after CO_2–water–oil–rock interaction for core No. 3 slice (S_{wr} = 0.5) (reaction time, 16 days): (**a**, **c**, **e**, **g**) calcite, feldspar, chlorite, kaolinite before reaction; (**b**, **d**, **f**, **h**) calcite, feldspar, chlorite, kaolinite after reaction; (**i**, **j**) pore structures before and after reaction.

$$\text{Chlorite}: [Fe/Mg]_5Al_2Si_3O_{10}(OH)_8 + 5CaCO_3 + 5CO_2 \leftrightarrow 5Ca[Fe/Mg](CO_3)_2 + Al_2Si_2O_5(OH)_4 + SiO_2 + 2H_2O \quad (13)$$

Analysis of XRD results of the mineral composition of cores No. 2 (oil-saturated) and No. 3 (S_{wr} = 0.5) before and after the CO_2–water–oil–rock interactions are shown in Fig. 13. The calcite and feldspar are primarily dissolved within the cores, while the minerals of kaolinite and quartz precipitate during the process of CO_2 flooding and storage. Compared with core No. 2 slice, the CO_2–water–rock reaction for core No. 3 slice is more significant. In terms of the XRD spectrum of the core No. 2 slice, the diffraction peak heights of feldspar have decreased by 1.2%, whereas the peak

heights of kaolinite and quartz have increased by 0.9% and 1.3%, respectively. However, the peak heights of feldspar in the XRD spectrum of core No. 3 slice (Fig. 13(b)) decreased by 2.5%, while the peak heights of quartz and kaolinite increased by 2.4% and 1.5%, respectively after the reaction. After the CO_2–water–rock reaction, core No. 3 exhibits an increment of porosity of 6.2% and permeability of 0.96 mD, while core No. 2, after the CO_2–water–oil–rock reaction, its porosity and permeability increase by 4.3% and 0.51 mD, respectively. These changes indicate the CO_2–water–rock reaction is more intense when the water saturation of the reservoir is higher, which improves the reservoir properties such as porosity, permeability, and wettability. Consequently, this CO_2–water–oil–rock reaction enhances both the CO_2-enhanced oil recovery (EOR) and the enhanced CO_2 sequestration (ECS) effect in reservoirs.

5. Discussion

5.1. Effect of pressure on CO_2 displacement and sequestration

Fig. 14 illustrates the impact of CO_2 injection pressure on CO_2-EOR and ECS of micropores of reservoirs. As the CO_2 injection pressure rises from 10 to 15 MPa, the pore size threshold for oil production decreases from 0.08 to 0.04 μm with an incremental oil recovery of 7.6%, and the T_2 spectrum exhibits a corresponding reduction. This suggests that both the efficiency of oil recovery and the quantity of CO_2 sequestration within the core are significantly improved. The increase in the pressure of CO_2 injection promotes the mass transfer between CO_2 and formation oil, thereby inducing a reduction in IFT, which facilitates the entry of more CO_2 into smaller pores for displacing oil and being trapped within the pores. The CO_2 dissolution amount in oil is also enhanced with the increase of CO_2 injection pressure, which reduces the viscosity of oil, swells the oil, and improves the oil recovery in larger pores.

As a comparison, the effect of CO_2-EOR and ECS in core No. 2 (S_{wr} = 0.5) is shown in Fig. 15. As the CO_2 injection pressure increases from 10 to 15 MPa, the pore size threshold for oil production decreases from 0.07 to 0.05 μm with an incremental oil recovery 5.3%. The reduction increment of the pore size threshold for oil production and CO_2 sequestration with this core is lower than that with oil-saturated cores with the CO_2 injection pressure increase. The primary reason for this phenomenon can be attributed to the isolating effect of the water wall formed in reservoir pores, which isolates the CO_2 within the larger pores with the oil in the smaller pores, resulting in an increase in the resistance of CO_2 entering the small pores for oil displacement.

The analysis of the NMR images of cores (oil-saturated and

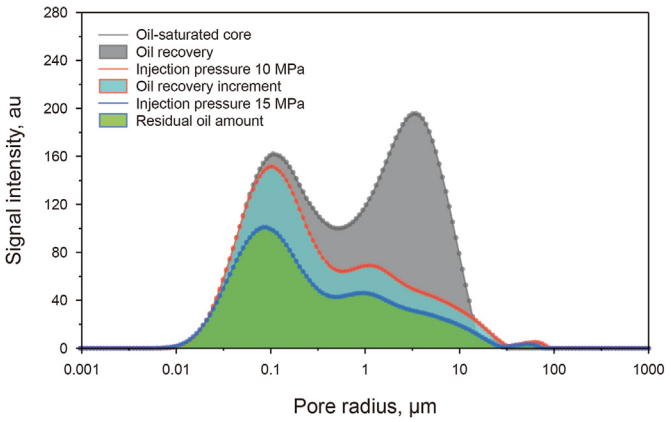


Fig. 14. Effect of CO_2 displacement and sequestration in micropores of the oil-saturated core No. 2 by CO_2 immiscible displacement at different CO_2 injection pressure (time = 120 min).

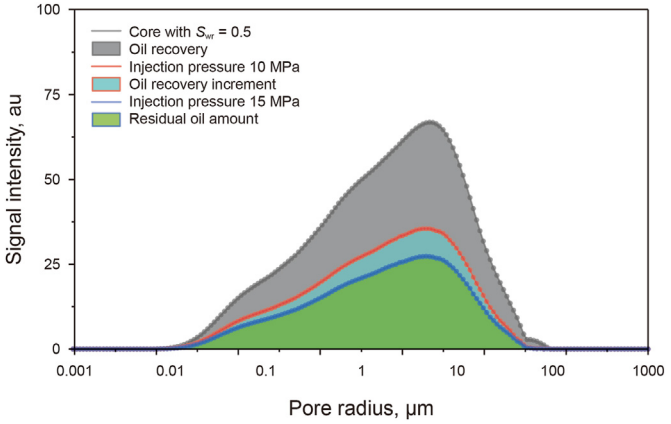


Fig. 15. Effect of CO_2 displacement and sequestration in micropores of the core No. 2 (S_{wr} = 0.5) by CO_2 immiscible displacementat different CO_2 injection pressure (time = 120 min).

S_{wr} = 0.5) tested at different time nodes, shown in Fig. 16, reveals that the oil recovery for all cores will increase with the increase in CO_2 injection pressure. Additionally, the amount of CO_2 sequestration (structural and residual sequestration) by replacing fluids within reservoir pores is the highest among all sequestration mechanisms. However, the CO_2-EOR effect on the core (S_{wr} = 0.5) is better than that on the oil-saturated core. The reason for improved

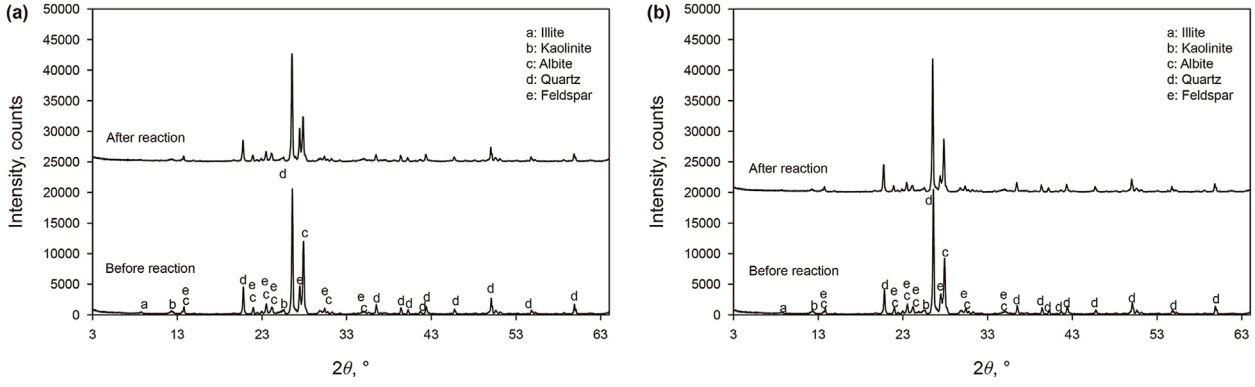


Fig. 13. XRD spectrum of mineral composition of experimental core slices: (**a**) oil-saturated core No. 2 slice; (**b**) core No. 3 slice (S_{wr} = 0.5).

EOR with the increase of CO_2 injection pressure was the CO_2 dissolution and diffusion into oil and water was accelerated with the increased injection pressure, resulting in more CO_2 dissolution into the oil and water phases, which resulted in a lower IFT. However, the reduction in IFT between the CO_2 and oil phases is more significant than that between CO_2 and the water phase, ultimately leading to a larger decrease in capillary resistance for the oil-saturated core as the injection pressure of CO_2 increases.

5.2. Effect of residual water saturation on CO_2 displacement and sequestration

After 16 days of reaction of CO_2 with the slice of core No. 2 (oil-saturated) and the slice of core No. 3 ($S_{wr} = 0.5$), the contact angles of the water phase on the rock surfaces of the two core slices decreased from 125.3° to 116.7° and from 123.7° to 69°, respectively (see Fig. 17). The finding suggests that the hydrophilicity of the core No. 3 slice has surpassed that of the core No. 2 slice, indicating the reaction degree of CO_2–water–rock is enhanced with the increase of the S_{wr} of reservoirs. The rise of the hydrophilicity of reservoir pores is beneficial for CO_2 entering into the smaller pores for oil displacement and adhesive oil droplets detaching from the rock surface, which improves the CO_2-EOR. Similar research conclusions can also be found in elsewhere (Iglauer, 2017; Li et al., 2016; Wenzel, 1949). The authors established a correlation between the wettability of rock and the roughness of its surface, as demonstrated in Eq. (14). Their findings indicate that the CO_2–water–rock reaction has the potential to enhance the roughness of the rock surface, decrease the contact angle of the water phase, and thereby promote the hydrophilic properties of the surface. Through the XRD test of the core slices before and after reactions combined with the reaction Eqs. (11)–(13), more hydrophilic minerals (kaolinite and quartz) are formed within the core after the CO_2-induced reaction, which also resulted in an enhancement of the hydrophilicity of the rock surface. Zhang et al. (2018) also observed similar mineral and wettability evolution on the surface of cores through CO_2–water–rock reaction experiments combined with the contact angle test for cores before and after the CO_2–water–rock reaction.

$$\cos\theta_r = \gamma\cos\theta_s \tag{14}$$

where θ_r is the contact angle of the water phase on the rock surface after the CO_2–water–rock reaction, °; θ_s is the contact angle of the water phase on an ideal rock surface, °; γ is the roughness ratio.

The oil recovery and CO_2 sequestration ratio within the micropores for the oil-saturated core No. 2 before and after the CO_2–water–oil–rock interaction are shown in Fig. 18. Following a sixteen-day reaction period, the core was re-saturated with oil and repeatedly flooded with CO_2 through immiscible injection. Comparison of NMR spectra of the core after the first oil-saturated and CO_2 displacement, the area of the NMR spectrum curves for the same core after re-oil-saturation and CO_2 displacement increases and decreases by 1.5% and 0.39%, respectively. The area of the NMR T_2 spectrum characterizes the oil content in the pores of the tested

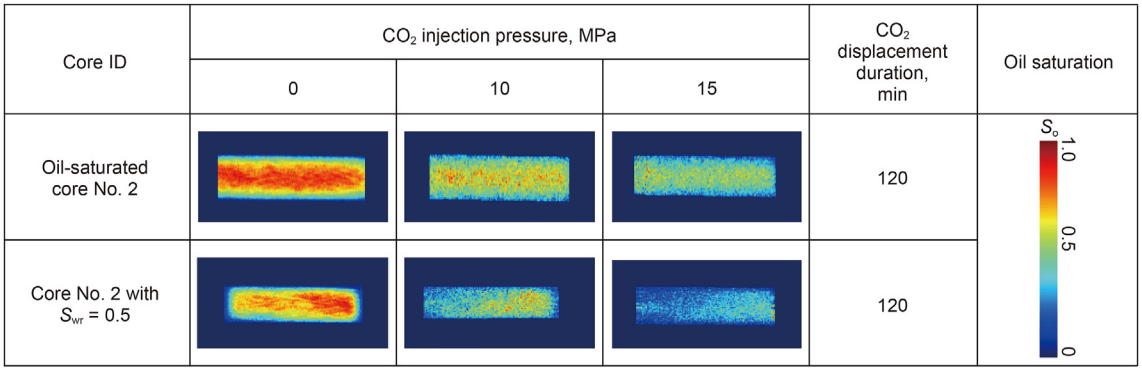


Fig. 16. Comparison of NMR images of residual oil in different S_{wr} cores at different stages of CO_2 displacement.

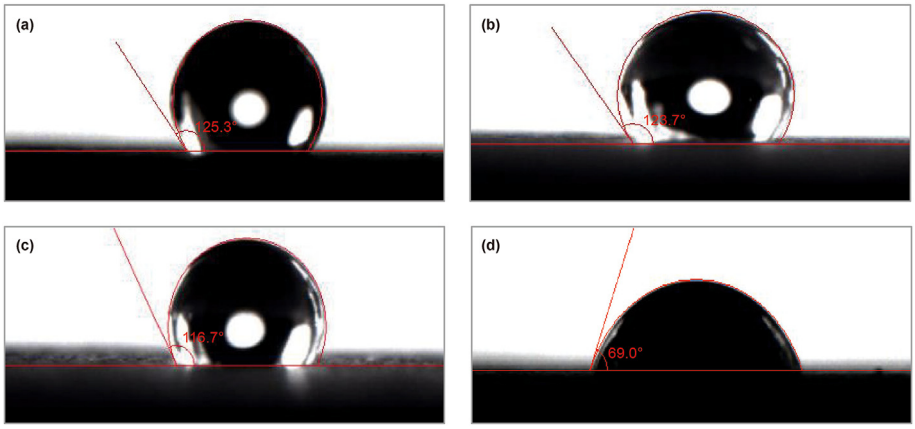


Fig. 17. Contact angles of core slices before (top) and after (bottom) CO_2–water–oil–rock interactions: (**a**, **b**) contact angle of the water phase of the dried cores No. 2 and No. 3 slices, respectivley, before reaction; (**c**) contact angle of the water phase of the oil-saturated core No. 2 slice after CO_2–water–oil–rock reaction (the core after washing oil and drying); (**d**) contact angle of the water phase of core No. 3 slice with residual water saturation $s_{wr} = 0.5$ after CO_2–water–oil–rock reaction (the core after washing oil and drying).

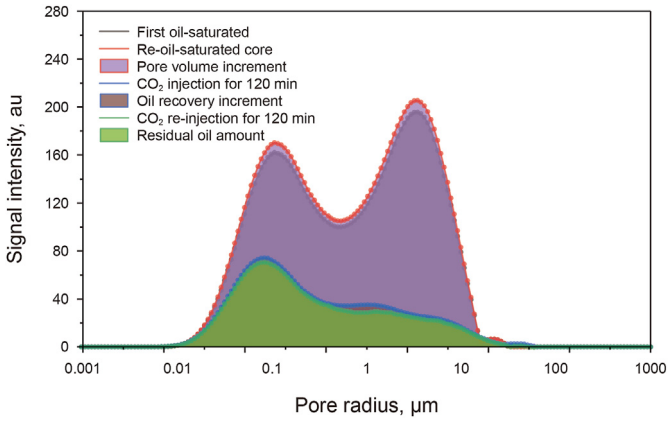


Fig. 18. Changes of oil production and CO_2 sequestration in micropores of the core No. 2 before and after CO_2–water–rock interaction (pressure = 15 MPa).

core. The increase of T_2 spectrum area for the re-oil-saturated core indicates more oil is saturated into the pores of the core, which reveals the pore volume of the core is increased after the first CO_2 displacement. The reduction of the T_2 spectrum area after CO_2 re-injection indicates more oil is produced, which also reveals that the CO_2–water–rock interaction not only increases the pore volume but also improves the seepage ability of fluids in the core, thereby enhancing the CO_2-EOR and ECS effect.

6. Conclusions

The coupled effect of CO_2-enhanced oil recovery and CO_2 sequestration within micropores of reservoirs is mainly related to factors such as reservoir water saturation, CO_2 injection pressure, and CO_2–water–oil–rock interaction, which affects mass transfer, IFT between oil and CO_2, and the wettability of rock. The research results help reveal the changing patterns of reservoir properties and understand the microscopic mechanisms of oil extraction and CO_2 sequestration in different scales of micropores after CO_2 injection into low-permeable reservoirs with different water saturation and provide theoretical references for applications of CO_2-EOR and sequestration on-site scale. Based on the experimental results, the following conclusions are drawn.

(1) The CO_2 sequestration effect in reservoirs is positively correlated with CO_2-EOR, accounting for over 50% of the reservoir pore volume. The increase in CO_2 injection pressure can reduce the pore size threshold of produced oil from smaller pores, which promotes the improvement of oil recovery. Furthermore, the CO_2 sequestration effect within reservoirs is also improved because more fluids within reservoir pores are replaced by the higher pressure of CO_2 injection.

(2) CO_2 can enter into the smaller pores to displace oil with the reduction of reservoir water saturation. In theory, the oil recovery and CO_2 sequestration effect with the oil-saturated cores after CO_2 injection will be better. However, the oil recovery and CO_2 sequestration ratio is higher with cores with $S_{wr} = 0.5$. We thought three reasons could lead to this. Firstly, CO_2 breakthrough is more severe in oil-saturated cores. In addition, the improvement effect of hydrophilicity of cores ($S_{wr} = 0.5$) after CO_2 injection is better, which reduces the adhesion work of CO_2 stripping formation oil on the rock surface. Lastly, the oil content in small pores of oil-saturated cores is higher, which also leads to low oil recovery by CO_2 immiscible flooding.

(3) The increase in water saturation in the reservoir promotes the contact between the formation water, CO_2, and rocks, thereby facilitating the occurrence of reactions. Therefore, the improved hydrophilicity of the rock surface and the pore volume increment of the cores is better for the cores ($S_{wr} = 0.5$) than that of the oil-saturated cores. This also indicates that low-permeable reservoirs with a certain water saturation are more suitable for CO_2 immiscible flooding to improve CO_2 displacement and sequestration effect.

The mechanisms and induced factors of the microscopic CO_2-EOR and ECS after CO_2 injection into reservoirs are clarified in this paper. Further sensitivity analysis of the impact of the water saturation of reservoirs on the microscopic effects of CO_2 displacement and sequestration is meaningful for making a suitable CO_2 injection strategy. The mutual verification research between numerical simulations at site scales and experiments of CO_2 flooding and sequestration under different CO_2 injection methods needs to be undertaken.

CRediT authorship contribution statement

Ming-Xing Bai: Writing – review & editing, Funding acquisition. **Zhi-Chao Zhang:** Writing – original draft, Formal analysis, Data curation, Conceptualization. **Er-Long Yang:** Validation, Methodology, Conceptualization. **Si-Yu Du:** Methodology, Investigation.

Declaration of competing interest

The authors declare that they have no known competing financial interests or personal relationships that could have appeared to influence the work reported in this paper.

Acknowledgments

This work is supported by the National Key Research and Development Program of China, China (Grant No.: 2022YFE0206700) and the National Natural Science Foundation of China, China (Grant No.: 52474035). Furthermore, the authors would like to thank all members of the research team.

References

Ampomah, W., Balch, R., Will, R., et al., 2017. Co-optimization of CO_2-EOR and storage processes under geological uncertainty. Energy Proc. 114, 6928–6941. https://doi.org/10.1016/j.egypro.2017.03.1835.

Arsyad, A., Mitani, Y., Babadagli, T., 2013. Comparative assessment of potential ground uplift induced by injection of CO_2 into Ainoura, and Berea sandstone formations. Earth Planet. Sci. 6, 278–286. https://doi.org/10.1016/j.proeps.2013.01.037.

Assef, Y., Apostolos, K., Almao, P.P., 2019. Numerical modelling of cyclic CO_2 injection in unconventional tight oil resources; trivial effects of heterogeneity and hysteresis in Bakken formation. Fuel 236, 1512–1528. https://doi.org/10.1016/j.fuel.2018.09.046.

Benson, S.M., Deutch, J., 2018. Advancing enhanced oil recovery as a sequestration asset. Joule 2 (8), 1386–1389.

Brown, K., Whittaker, S., Wilson, M., et al., 2017. The history and development of the IEA GHG Weyburn-Midale CO_2 Monitoring and Storage Project in Saskatchewan, Canada (the world largest CO_2 for EOR and CCS program). Petroleum 3 (1), 3–9. https://doi.org/10.1016/j.petlm.2016.12.002.

Bui, M., Adjiman, C.S., Bardow, A., et al., 2018. Carbon capture and storage (CCS): the way forward. Energy Environ. Sci. 11 (5), 1062–1176. https://doi.org/10.1039/C7EE02342A.

Cui, G., Yang, L., Fang, J., et al., 2021. Geochemical reactions and their influence on petrophysical properties of ultra-low permeability oil reservoirs during water and CO_2 flooding. J. Petrol. Sci. Eng. 203, 108672. https://doi.org/10.1016/j.petrol.2021.108672.

Davarpanah, A., Mirshekari, B., 2020. Experimental study of CO_2 solubility on the oil

recovery enhancement of heavy oil reservoirs. J. Therm. Anal. Calorim. 139, 1161–1169. https://doi.org/10.1007/s10973-019-08498-w.
Fan, L., Chen, J., Zhu, J., et al., 2022. Experimental study on enhanced shale oil recovery and remaining oil distribution by CO_2 flooding with Nuclear Magnetic Resonance technology. Energy Fuels 36 (4), 1973–1985. https://doi.org/10.1021/acs.energyfuels.1c02982.
Gao, R., Lv, C., Lun, Z., et al., 2021. Integrated evaluation method of CO_2 flooding and storage. Therm. Power Gener. 50 (1), 115–122 (in Chinese).
Global CCS Institute, 2021. Global Status of CCS Report 2020. Melbourne, Australia.
He, L., Shen, P., Liao, X., et al., 2016. Potential evaluation of CO_2 EOR and sequestration in Yanchang oilfield. J. Energy Inst. 89 (2), 215–221. https://doi.org/10.1016/j.joei.2015.02.002.
Hu, Y., Hao, M., Chen, G., et al., 2019. Technologies and practice of CO_2 flooding and sequestration in China. Petrol. Explor. Dev. 46 (4), 716–727. https://doi.org/10.1016/S1876-3804(19)60233-8.
IEA, 2020. Energy Technology Perspectives 2020: Special Report on Carbon Capture, Utilization and Storage. Paris.
Iglauer, S., 2017. CO_2–water–rock wettability: variability, influencing factors, and implications for CO_2 geostorage. Acc. Chem. Res. 50 (5), 1134–1142. https://doi.org/10.1021/acs.accounts.6b00602.
Kashkooli, S., Gandomkar, A., Riazi, M., et al., 2022. Coupled optimization of carbon dioxide sequestration and CO_2 enhanced oil recovery. J. Pet. Sci. Eng. 208, 109257. https://doi.org/10.1016/j.petrol.2021.109257.
Khurshid, I., Afgan, I., 2021. Geochemical investigation of CO_2 injection in oil and gas reservoirs of middle east to estimate the formation damage and related oil recovery. Energies 14 (22), 7676 ttps://doi.org/10.3390/en14227676.
Koottungal, L., 2014. 2014 worldwide EOR survey. Oil Gas J. 112 (4), 79–91.
Lai, J., Wang, G., Wang, Z., et al., 2018. A review on pore structure characterization in tight sandstones. Earth Sci. Rev. 177, 436–457. https://doi.org/10.1016/j.earscirev.2017.12.003.
Le, N.N.H., Sugai, Y., Vo-Thanh, H., et al., 2022. Experimental investigation on plugging performance of CO_2 microbubbles in porous media. J. Pet. Sci. Eng. 211, 110187. https://doi.org/10.1016/j.petrol.2022.110187.
Li, B., Ye, J., Li, Z., et al., 2016. Phase interaction of CO_2-oil-water system and its effect on interfacial tension at high temperature and high pressure. Acta Pet. Sin. 37 (10), 1265–1272. https://doi.org/10.7623/syxb201610006 (in Chinese).
Li, D.C., Saraji, S., Jiao, Z., et al., 2021. CO_2 injection strategies for enhanced oil recovery and geological sequestration in a tight reservoir: an experimental study. Fuel 284, 119013. https://doi.org/10.1016/j.fuel.2020.119013.
Liu, Z.X., Gao, M., Zhang, X.M., et al., 2023. CCUS and CO_2 injection field application in abroad and China: status and progress. Geoenergy Sci. Eng. 229, 212011. https://doi.org/10.1016/j.geoen.2023.212011.
Preston, C., Monea, M., Jazrawi, W., et al., 2005. IEA GHG Weyburn CO_2 monitoring and storage project. Fuel Process. Technol. 86 (14–15), 1547–1568. https://doi.org/10.1016/j.fuproc.2005.01.019.
Page, B., Turan, G., Zapantis, A., et al., 2020. The Global Status of CCS 2020: Vital to Achieve Net Zero. Global CCS Institute, Melbourne.
Rathnaweera, T.D., Ranjith, P.G., Perera, M.S.A., 2016. Experimental investigation of geochemical and mineralogical effects of CO_2 sequestration on flow characteristics of reservoir rock in deep saline aquifers. SCI Rep-UK 6, 19362. https://doi.org/10.1038/srep19362.
Saidian, M., Prasad, M., 2015. Effect of mineralogy on nuclear magnetic reso-nance surface relaxivity: a case study of Middle Bakken and Three Forks formations. Fuel 161, 197–206. https://doi.org/10.1016/j.fuel.2015.08.014.
Steel, L., Liu, Q., Mackay, E., et al., 2016. CO_2 solubility measurements in brine under reservoir conditions: a comparison of experimental and geochemical modeling methods. Greenhouse Gases. Sci. Technol. 6 (2), 197–217. https://doi.org/10.1002/ghg.1590.
Wang, H., Lun, Z., Lv, C., et al., 2018. Nuclear-magnetic-resonance study on mechanisms of oil mobilization in tight sandstone reservoir exposed to carbon dioxide. SPE J. 23, 750–761. https://doi.org/10.2118/179554-PA.
Wang, H., Ji, B., Zhao, S., et al., 2022. Feasibility study on the CO_2 flooding and storage in the complex fault-block tight oil reservoir. J. Shaanxi Univ. Sci. Technol. Nat. Sci. Ed. 40 (3), 115–122 (in Chinese).
Wei, B., Gao, H., Pu, W., et al., 2017. Interactions and phase behaviors between oleic phase and CO_2 from swelling to miscibility in CO_2-based enhanced oil recovery (EOR) process: a comprehensive visualization study. J. Mol. Liq. 232, 277–284. https://doi.org/10.1016/j.molliq.2017.02.090.
Wenzel, R.N., 1949. Surface roughness and contact angle. J. Phys. Chem. 53 (9), 1466–1467. https://doi.org/10.1021/j150474a015.
Whorton, L.P., Eugene, R.B., Alvin, B.D., 1952. Method for producing oil by means of carbon dioxide. U.S. Patent No. 2,623,596.
Yang, D., Gu, Y., Tontiwachwuthikul, P., 2008. Wettability determination of the reservoir brine–reservoir rock system with dissolution of CO_2 at high pressures and elevated temperatures. Energy Fuels 22 (1), 504–509. https://doi.org/10.1021/ef700383x.
Yang, P., Guo, H., Yang, D., 2013. Determination of residual oil distribution during waterflooding in tight oil formations with NMR relaxome-try measurement. Energy Fuels 27 (10), 5750–5756. https://doi.org/10.1021/ef400631h.
Yao, Y.D., Li, X.F., 2009. A Study on CO_2 flooding effectiveness and its geologic storage. Xinjing Pet. Geol. 30 (4), 493–495 (in Chinese).
Yuan, S.Y., Ma, D., Li, J., et al., 2022. Progress and prospects of carbon dioxide capture, EOR-utilization and storage industrialization. Petrol. Explor. Dev. 49 (4), 955–962. https://doi.org/10.1016/S1876-3804(22)60324-0.
Zhang, X., Wei, B., Shang, J., et al., 2018. Alterations of geochemical properties of a tight sandstone reservoir caused by supercritical CO_2-brine-rock interactions in CO_2-EOR and geosequestration. J. CO_2 Util. 28, 408–418. https://doi.org/10.1016/j.jcou.2018.11.002.
Zhang, Y., Gao, M., You, Q., et al., 2019. Smart mobility control agent for enhanced oil recovery during CO_2 flooding in ultra-low permeability reservoirs. Fuel 241, 442–450. https://doi.org/10.1016/j.fuel.2018.12.069.
Zhang, Z., Bai, M., Xu, L., et al., 2024a. Study on oil extraction characteristics in micropores of a typical terrestrial shale reservoir in China by CO_2 injection and surfactant imbibition. Energy Fuels 38 (8), 6927–6937. https://doi.org/10.1021/acs.energyfuels.4c00330.
Zhang, Z., Bai, M., Xu, L., et al., 2024b. Investigation on the impact of CO_2-induced precipitation on microscopic pore structure of low-permeable reservoirs. Geoenergy Sci. Eng. 213441. https://doi.org/10.1016/j.geoen.2024.213441.
Zhao, F., Hao, H., Hou, J., et al., 2015. CO_2 mobility control and sweep efficiency improvement using starch gel or ethylenediamine in ultra-low permeability oil layers with different types of heterogeneity. J. Pet. Sci. Eng. 133, 52–65. https://doi.org/10.1016/j.petrol.2015.05.014.
Zhao, Q., Lun, Z., Zhang, X., et al., 2019. Mechanism of shale oil mobilization under CO_2 injection. Oil Gas Geol. 40, 1333–1338 (in Chinese).
Zhou, X., Yu, W., Lei, G., et al., 2024. Experimental study on dual benefits of improvement of CO_2 enhanced oil recovery and its storage capacity for depleted carbonate oil reservoirs. Adv. Geo-Energy Res. 12 (1), 52–65. https://doi.org/10.46690/ager.2024.04.05.